Single-Cell Level Raman Molecular Profiling Reveals the Classification of Growth Phases of Chaetoceros tenuissimus

Single-cell Level Raman Molecular Profiling Reveals the Classification of Growth Phases of *Chaetoceros tenuissimus*.

Masahiro Ando[a,$], Kaori Sugiyama[b,$], Koya Kubo[c,d,$], Shumpei Horii[c,d], Takeshi Hano[e], Yuji Tomaru[e], Haruko Takeyama[a,b,c,d,f,*]

[a] Research Organization for Nano and Life Innovation, Waseda University, 513 Wasedatsurumaki-Cho, Shinjuku-Ku,Tokyo, 169-0041, Japan

[b] Institute for Advanced Research of Biosystem Dynamics, Waseda Research Institute for Science and Engineering, Waseda University, 3-4-1 Okubo, Shinjuku-Ku, Tokyo, 169-8555, Japan

[c] Department of Advanced Science Engineering, Graduate School of Advanced Science and Engineering, Waseda University, 3-4-1 Okubo, Shinjuku-Ku, Tokyo, 169-8555, Japan

[d] Computational Bio Big-Data Open Innovation Laboratory, AIST-Waseda University, 3-4-1 Okubo, Shinjuku-Ku, Tokyo, 169-8555, Japan

[e] Environment Conservation Division, Fisheries Technology Institute, National Research and Development Agency, Japan Fisheries Research and Education Agency, 2-17-5 Maruishi, Hatsukaichi, Hiroshima, 739-0452, Japan

[f] Department of Life Science and Medical Bioscience, Waseda University, 2-2 Wakamatsu-cho, Shinjuku-ku, Tokyo 162-8480, Japan

*Email: haruko-takeyama@waseda.jp

[$]*M.A., K.S., and K.K. contributed equally to this paper.*

Abstract

Harmful algal blooms (HABs) are a natural phenomenon caused by outbreaks of algae, resulting in serious problems for aquatic ecosystems and the coastal environment. *Chaetoceros tenuissimus* (*C. tenuissimus*) is one of the diatoms responsible for HABs. The growth curve of C.tenuissimus can be observed from beginning to end of HABs, therefore, detailed analysis is necessary to characterize each growth phase of *C. tenuissimus*. It is important to examine the phenotype of each diatom cell individually, as they display heterogeneity even in the same growth phase. Raman spectroscopy is a label-free technique to elucidate biomolecular profiles and spatial information at the cellular level. Multivariate data analysis (MVA) is an efficient method for the analysis of complicated Raman spectra, to identify molecular features. Here, we utilized Raman microspectroscopy to identify the molecular information of each diatom cell, at the single-cell level. The MVA, together with a Support Vector Machine (SVM), which is a machine learning technique, allowed the classification of proliferating and non-proliferating cells. The classification includes polyunsaturated fatty acids such as linoleic acid, eicosapentaenoic acid (EPA), and docosahexaenoic acid (DHA). This study indicated that Raman spectroscopy is an appropriate technique to examine *C. tenuissimus* at the single-cell level, providing relevant data to assess the correlation between the molecular details obtained from the Raman analysis, at each growth phase.

Introduction

Harmful algal blooms (HABs) are caused in various coastal areas and have a serious impact on coastal environments and fishing industry. Therefore, it is important to understand the state of their proliferation and to predict whether the bloom will continue or disappear. Recent research has been conducted to elucidate the causes and dynamics of HABs and to identify the exact species involved [1]. Phytoplankton, including dinoflagellates and diatoms, are known to cause HABs.

Diatoms are categorized as unicellular, photosynthetic, eukaryotic algae, which live in aquatic environments throughout the world. Diatoms account for 35-75% of primary production in the oceans. They form the base of the food web and support coastal fisheries as a source of nutrients for secondary consumers [2]. *Chaetoceros*, is a highly diverse genus, comprised of over 400 species of small marine diatoms, which are believed to play an important role in primary production [3]. Among this genus, *Chaetoceros tenuissimus* (*C. tenuissimus)* is an international marine diatom found in areas such as Narragansett Bay, the Mediterranean Sea, and San Mathias Gulf [4], and which often appears in large numbers in Hiroshima Bay, in Japan, during warm weather [5] . These large outbreaks cause major fishing problems in Japan.

Gas Chromatography-Mass Spectrometry (GC-MS) and High-Performance Liquid Chromatography (HPLC) are frequently used for metabolite analysis in algae and have also been utilized as a biomarker to detect mannuronic acids, in the stationary growth phase of *C. tenuissimus* [4]. Liquid Chromatography-Tandem Mass Spectrometry has been performed to measure the changes in metabolites of the marine diatom *Pseudo-nitzschia multistriata*, during sexual reproduction process [6]. However, sample preparation for mass spectrometry is time-consuming and cannot perform measurements at the single-cell level. The microbial population of the marine diatom is known to be phenotypically variable and heterogeneous in each cell, depending on the environment[7] . Therefore, comprehensive methods for obtaining molecular

information at the single-cell level are required to elucidate the diversity of individual diatom cells at each growth phase.

Raman spectroscopy produces spectra which illustrate the photon-scattering intensity of molecular vibrations, revealing the molecular structure and crystalline state of a substance. Previous Raman spectroscopic studies on algae include the identification of dominant species in mass algal populations, using Confocal Resonance Raman Spectroscopy [8], and the elucidation of carotenoid composition differences in each cell line of *Chlamydomonadales* [9] . However, these studies focused on the Raman bands specific to each component, and it is difficult to distinguish components when the Raman bands of the target compounds overlap.

Multivariate Curve Resolution-Alternating Least Squares analysis (MCR-ALS), is a multivariate data analysis method, used to decompose data sets into component spectra and their intensity information. The combination of Raman spectroscopy and MCR-ALS is utilized to reveal the details of molecular features. Since the Raman spectrum is non-negative conditioned, using MCR-ALS it is possible to extract target spectral components, even if some Raman bands overlap with other molecular components. Previous studies combining Raman spectroscopy and MCR-ALS include the detection of intracellular Penicillin G at the single-cell level [10], the identification of disease-specific Raman marker spectral components [11], and the elucidation of the diversity of the water spectrum derived from biocomponent-specific hydration structures [12]. In this study, we performed Raman spectroscopy for *C. tenuissimus* to determine the growth phase of diatoms at the single-cell level. Semi-quantitative analysis of Raman spectra with MCR-ALS was conducted to elucidate the growth phase-dependent components of the diatoms, which are dependent, not only on the specific growth phase, but also on pervasive biocomponents.

Experimental Methods

Diatom Preparations

Chaetoceros tenuissimus, which is a clonal axenic strain (NIES-3715, formerly 2-10), was used in this study and cultured with SWM-3 medium [13,14]. The cells were maintained under a 12:12 h, light/dark regime at 25°C. For Raman measurements, cells were collected each day from day2 to day8 of and measured by Confocal Raman microspectroscopy.

Raman Spectroscopy Measurements

The Confocal Raman microspectroscopy procedures used, were those reported by Horii et al., 2023, using a 100x, 1.4-N.A. objective lens. The spatial resolutions of the microscopic system are ~0.3 µm in lateral direction and 1.5 µm in depth direction. Several chemical reagents were prepared to measure the Raman spectra, namely tripalmitin (FUJIFILM Wako Pure Chemical Corp., Tokyo, Japan), palmitoleic acid (FUJIFILM Wako Pure Chemical Corp., Tokyo, Japan), linoleic acid (FUJIFILM Wako Pure Chemical Corp., Tokyo, Japan), eicosatetraenoic acid (EPA) (FUJIFILM Wako Pure Chemical Corp., Tokyo, Japan), docosahexaenoic acid (DHA) (FUJIFILM Wako Pure Chemical Corp., Tokyo, Japan), glucose (FUJIFILM Wako Pure Chemical Corp., Tokyo, Japan), cellobiose (FUJIFILM Wako Pure Chemical Corp., Tokyo, Japan), and mannose (FUJIFILM Wako Pure Chemical Corp., Tokyo, Japan). These reagents were placed in a coverslip (Matsunami Glass Ind., Osaka, Japan).

Single point measurements were conducted for each reagent and 20 spectra were taken at an acquisition time of 1 s per accumulation. A 20 mW laser was used with an excitation wavelength of 532 nm.

For Raman measurements of *C. tenuissimus*, at each time point, one drop of the cells was placed on the cell medium (Matsunami Glass Ind., Osaka, Japan) and protected by a coverslip. Raman mapping measures were performed using 32x32 µm – 40.25x40.25 µm with

0.25 μm step size, at an acquisition time of 1s per accumulation. Laser power was 4 mW. 1089-1764 Raman spectra were obtained from each diatom.

Raman Spectral Analysis

Raman spectral data were pretreated with the IGOR Pro software (WaveMetrics, Inc., Lake Oswego, OR, USA). Indene spectra were utilized for the wavenumber calibration standard. The halogen lamp spectra were used to calibrate the detector and the intensity. All spectra acquired in the Raman mapping measurements were combined into a single matrix, on which Singular Value Decomposition (SVD) was performed for noise reduction, prior to the MCR-ALS. The MCR-ALS methods employed by Ando et al. [15]were used, where the original data matrix (A) is decomposed into two matrices as given below.

$$\boldsymbol{A} \approx \boldsymbol{WH} \ (W, H \geq 0)$$

where $\boldsymbol{W}$ is the combined spectrum of the reference spectra, including the lipids, monosaccharides, the medium, and the SVD extracted spectra; and $\boldsymbol{H}$ is the intensity of each component.

The optimal solution was obtained using the additional linear constraint, l_1-norm regulation (Lasso regression) [16]. The hyperparameter λ, for Lasso regression, was determined to be 0.001 by cross validation. The initial value was based on the result of SVD and the standard spectra of biological components. Optimization allowed the use of an in-house program written in Python code [11,15]. The Raman images were analyzed using the $\boldsymbol{W}$ matrix and corresponding $\boldsymbol{H}$ matrix, with this program.

Molecular Prolife Analysis

From the intensity profile matrix, H, of the MCR-ALS, the sum of the intracellular component intensities in each data map was obtained. The sum of the intensities of each

biomolecular component was normalized to the sum of the intensities of the intracellular water components.

Principal component analysis (PCA) was performed on this data for cell classification. The supervised machine learning (SVM) method was used for classification and to determine the linear hyperplanes of the principal component plots. The teacher data for machine learning used the data from 48 hours of incubation and 192 hours of incubation. SVM can provide appropriate classification models, even for samples that cannot be linearly separated. However, in this study, a linear SVM was applied because linear data were used.

As another machine learning approach for cell classification, Random Forest analysis, was performed. Supervised learning was performed with 8:2 cross-validation using the intracellular intensity data from 48 hours of incubation and 192 hours of incubation, as the teacher data. All these analyses were performed with the Scikit-learn package in Python.

Results and Discussion

Growth Phase of *C. tenuissimus*

Based on the growth curves of *C. tenuissimus* cultures (Figure 1), growth phases were classified into lag phase (0-24 h), log phase (24-72 h), stationary phase (72-168 h), and death phase (after 168 h). To determine the growth phase-dependent phenotype of *C. tenuissimus*, cells were harvested at 48 h (log phase), 72, 96, 120, 168 h (stationary phase), and 192 h (death phase), and Raman mapping was performed on individual cells.

Molecular Component Extraction by Raman MCR-ALS Analysis

Single-cell Raman mapping measurements were performed to obtain molecular profiles of individual cells, at the single-cell level, at each incubation time. To determine the contribution of each biomolecular component from the Raman spectra, in which the spectra of various biocomponents overlap, a multivariate analysis method that can extract patterns of the entire spectrum of each biomolecular component is required, rather than a univariate analysis that focuses on a single band. In this study, MCR-ALS was used to extract biomolecular spectra and their intensity information, from the Raman spectra of *C. tenuissimus.*

Spectra of 13 components and their spatial intensity information are shown in Figure 2A and detailed band assignments are shown in Figure S1 and Table S1. Based on the comparison of Raman bands in accordance with the literature, the following molecular attributions are obtained. Components 1-5 were assigned to the standard spectra of tripalmitin, palmitoleic acid, linoleic acid, EPA, and DHA, respectively. Component 6 was assigned to polysaccharides and is characterized by 891 cm^{-1} derived from the C-H bending mode at the equatorial position[17]. Since diatoms produce a β-1,3 glucan-like molecule called chrysolaminaran[18], component 6 is predicted to be assigned to chrysolaminaran. The Raman spectrum of component 7 is assigned to a protein and is characterized by peaks at 1004 cm^{-1}, the ring-breathing mode of phenylalanine and tryptophan residues, 1442 cm^{-1} from C-H bending, and

1654 cm^{-1} from amide I[19]. Component 8 has strong Raman bands at 694 cm^{-1} and 1161 cm^{-1}, corresponding to P-O-P and PO^{2-} stretching of polyphosphate, respectively[20]. Finally, components 9-11 were assigned to the standard spectra of cellobiose, glucose, and mannose, respectively. In addition, spectra assigned to intracellular water molecules were also extracted, characterized by a broad Raman band at 1640 cm^{-1}, assigned to the O-H bending mode. From the above, the MCR-ALS decomposed the spectra of tripalmitin (1), palmitoleic acid (2), linoleic acid (3), EPA (4), DHA (5), polysaccharide (6), protein (7), polyphosphate (8), cellobiose (9), glucose (10), mannose (11), water (12), and Raman spectral components of the medium (13).

Intracellular molecular distribution images were constructed from the MCR-ALS analysis (Figure 2B). Polyunsaturated fatty acids such as linoleic acid, EPA, and DHA were confirmed to be localized in droplet form in the cells on Day 8 of the incubation time, which corresponds to the death phase. The Raman image of component 7 showed that the proteins were always distributed throughout the cell. However, since it is difficult to quantitatively determine the biological components specific to cells in the death phase, by Raman images alone, quantitative analysis utilizing intensity information of the intracellular component is needed.

Change Over Time in the Contribution of Each Biomolecular Component

The contribution of each molecular component and its change over time were evaluated from the intensity profile matrix of the MCR-ALS (Figure 3A). In each data map, the intensities of each molecular component were summed up within the cell and normalized to the total intensity of the water component. Analysis based on the signal intensity, relative to the amount of water, enables analysis that is independent of the detection sensitivity of the spectrometer and the sample.

Since EPA and DHA are both highly unsaturated fatty acid with 5 and 6 C=C double bounds, it was considered difficult to separate the exact contribution of each, so the normalized, total intensity of the two components was used as an indicator of ω3 fatty acids. As a result, it

was confirmed that the percentage of cells with high linoleic acid and ω3 fatty acid content increased between 120 and 192 hours of incubation. This is consistent with a previous study which reported that the diatom *Chaetoceros gracilis* increases the production of DHA only during the death phase [21]. This indicates that the production of unsaturated fatty acids such as linoleic acid and ω3 fatty acids increases with incubation time.

Linoleic acid is a molecule in the ω6 fatty acid synthesis pathway, but also acts as a substrate for α-linolenic acid, which is the basis for ω3 fatty acid synthesis. Therefore, the biosynthesis of linoleic acid may be activated for utilization as a substrate for the production of ω3 polyunsaturated fatty acids (Figure 3B). Variations in the content of linoleic acid and ω3 fatty acids were observed even in cells cultured for the same incubation time. This suggests that the growth stages of individual cells varied, even during the same incubation time, and that "proliferating" cells and "non-proliferating" cells were intermingled during each incubation time.

Cell Classification Based on the Biomolecular Profiles

As mentioned above, it was confirmed that the molecular profiles of the cells were diverse, even at the same incubation time. The growth curve is known to be represented by the average cellular state of the cell population, where there is the diversity in the proliferative state of the individual cells. Therefore, we attempted to identify the growth stage of individual cells at each incubation time by analysing the diversity of the molecular profiles of cells. The results of PCA using the intensity information of each molecule, obtained from MCR-ALS are shown in Figure 4A. The intensity information was obtained by summing up the intracellular intensities and normalizing them to the total intensity of the water component.

The PCA score plot showed that the distribution progressed in the same direction as incubation time: 2 days, 3-4 days, 5-7 days, and 8 days. The loadings of the principal components, which indicate the magnitude of the effect of each variable on the principal

components, suggested that linoleic acid, ω3 fatty acid, and palmitoleic acid were involved in this transition. For palmitoleic acid, the results are in agreement with a previous study [21] of *Chaetoceros gracilis*, one of the *Chaetoceros* species used in this study, in which palmitoleic acid was detected only in the exponential phase.

The distributions of cells at culture time 2 and culture time 8 can be differentiated from those present at culture times 3-7, whereas cells at culture times 3-7 were present across the distribution of both culture times. Here, 2, 3-7, and 8 incubation days correspond to the log, stationary, and death phases, respectively (Figure 4B). Therefore, the results indicate that the log phase is composed almost entirely of proliferating cells, and the death phase almost entirely of non-proliferating cells, while the stationary phase is a mixture of these cells. This indicates that the number of cells in the entire population has reached equilibrium.

We defined proliferating and non-proliferating cells at Day 2 and Day 8 of incubation, respectively, and attempted to discriminate them by machine learning, using these cells as teacher data. As a result, it was confirmed that the hyperplane of the SVM was determined by separating cells in the stationary phase. The fact that the hyperplanes were determined in a manner orthogonal to the direction of the main component loadings of linoleic acid, ω3 fatty acid, and palmitoleic acid, may support the hypothesis that the content of these molecules in individual cells changes according to their growth phase.

Similarly, we also attempted classification by Random Forest using intracellular component intensity information. The results also showed that proliferating and non-proliferating cells were clearly separated, and the major components contributing to the classification were linoleic acid, polyunsaturated fatty acids, and palmitoleic acid (Figure 4C and D). Consistent conclusions were obtained with two different machine learning methods, PCA-SVM and Random Forest, suggesting that it is possible to classify proliferating and non-proliferating cells by these fatty acids.

Determination of Growth Phase at Single Cell Level

The above results indicate that proliferating cells and non-proliferating cells are mixed in the stationary phase. We assumed that the proportion of proliferating and non-proliferating cells changes over time during the stationary phase. Therefore, from the PCA-SVD results, the proportion of the two classes of cells was compared with the actual incubation time (Figure 5A).

During the stationary phase, the percentage of proliferating cells was 100% on the 3rd day of culture, while the percentage of proliferating cells slightly decreased on the 4th and 5th day of culture. Furthermore, a significant increase in the percentage of non-proliferating cells was observed on the 7th day of culture. Comparing the growth curves with the population of proliferating cells, it was further revealed that there was little change in the growth curves between the mid and late stationary phase, but there was a significant decrease in the percentage of proliferating cells (Figure 5B).

This indicates that single-cell-level analysis of the growth stages of stationary phase cells can discriminate between the early, middle, and late stationary phases, which is difficult to do based on cell density alone. This suggests that analysis of molecular profiles at the single-cell level using Raman spectroscopy will enable us to predict the timing of occurrence of HABs.

Conclusion

In summary, we conducted Raman spectroscopy combined with multiple MVA to determine the growth phases of *C. tenuissimus* at the single-cell level. The death phase of *C. teneissimus* showed an increase of polyunsaturated fatty acid, such as linoleic acid, EPA, and DHA.

Raman spectra of *C. tenuissimus* was analyzed for each culture phase, revealing populations of proliferating and not-proliferating cells in the stationary phase. Single-cell Raman imaging of *C. tenuissimus* showed the different distribution of biomolecular components, including palmitoleic acid and polysaccharides in the periphery and center of the cells.

The SVM classification analysis reveals a decrease of log phase cells between the mid-stationary phase and end-stationary phase, with respect to proliferating and non-proliferating cells. These results indicated that single cell Raman spectroscopy of *C. tenuissimus* is able to categorize the cell phase between the mid-stationary phase and end-stationary phase, which is difficult to distinguish with cell density. This study has the potential use for the prediction of bloom demise.

Author Contributions

MA, KS, KK, SH, TH, YT, and HT conceived the idea and designed the experiments. KK, SH, and MA measured Raman spectra and analyzed the data. TH and YT prepared diatom cells and culture materials. MA wrote software Codes of MCR-ALS. MA, KS, KK and HT contributed to manuscript writing and all authors contribute discussion of content.

Acknowledgement

This work was supported by JSPS KAKENHI (grant number.JP7H06158).

Supporting Information

Raman band assignments of MCR-ALS decomposed spectra (DOC).

Figures

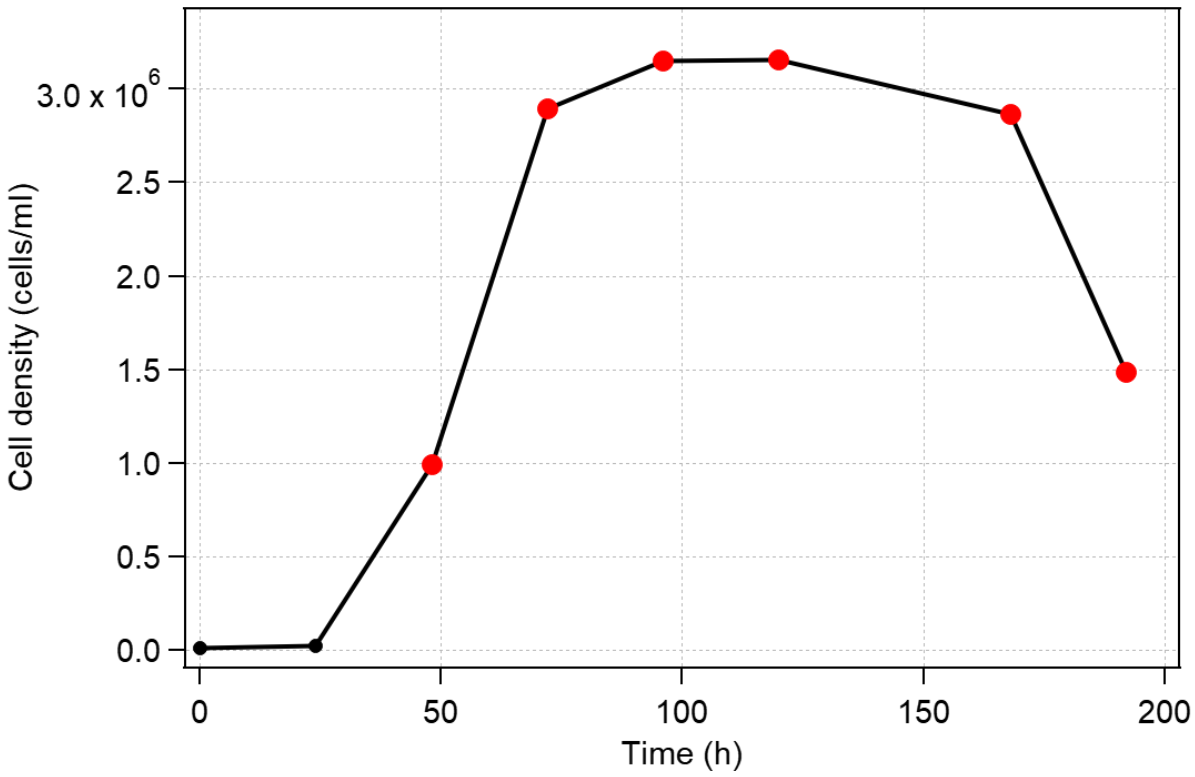

Figure 1. The growth curve of *C. tenuissimus*.

Raman measurements were conducted in 4 phases, including lag phase (0-24h), log phase (24-72h), stationary phase (72-168h), and death phase (after 168h) indicated in red.

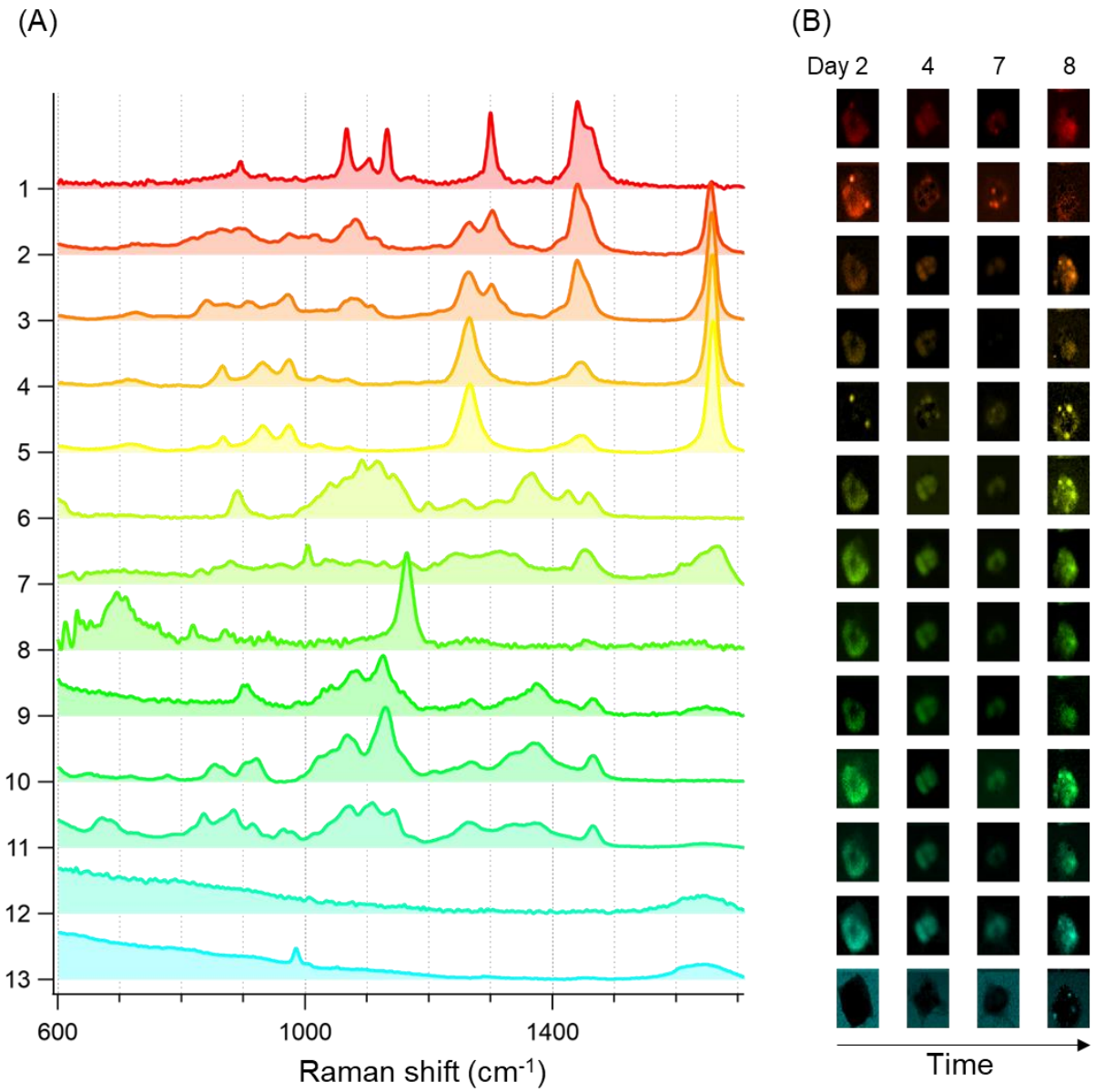

Figure 2. Raman spectra of molecular components and Raman images by MCR-ALS. (A) Decomposed Raman spectra of 13 components, including tripalmitin, palmitoleic acid, linoleic acid, EPA, DHA, polysaccharide, protein, polyphosphate, cellobiose, glucose, mannose, intracellular water, and cell culture medium. (B) Raman images of each component at day 2, 4, 7, and 8 after incubations.

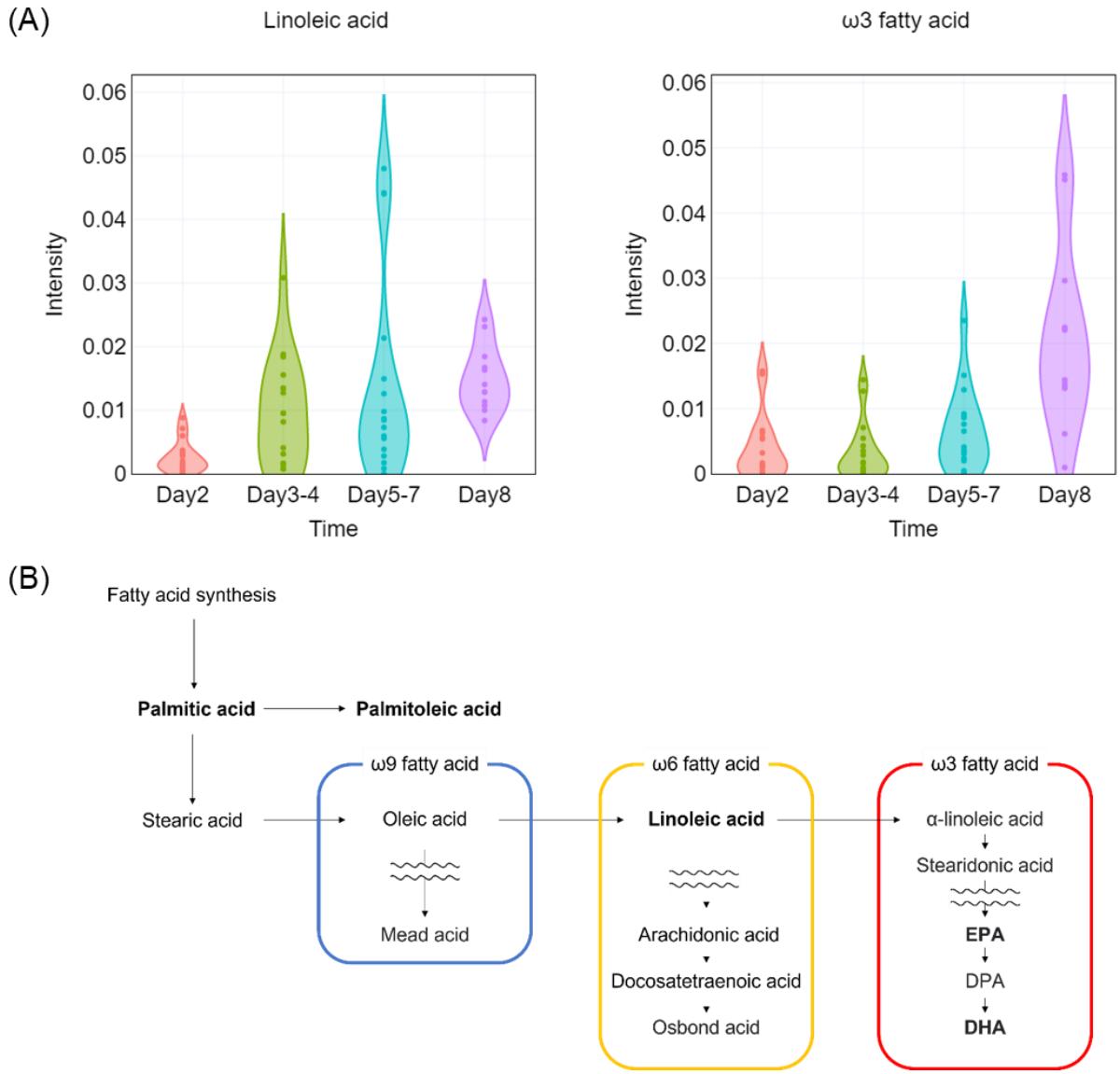

Figure 3. The changes of linolic acid and ω3 fatty acid during culture days and fatty acid synthesis pathway. (A) Linoleic acid ω3 fatty acids were observed and increased at day 8. (B) The fatty acid synthesis shows the ω3 fatty acids were derived from linoleic acid in ω6 fatty acid.

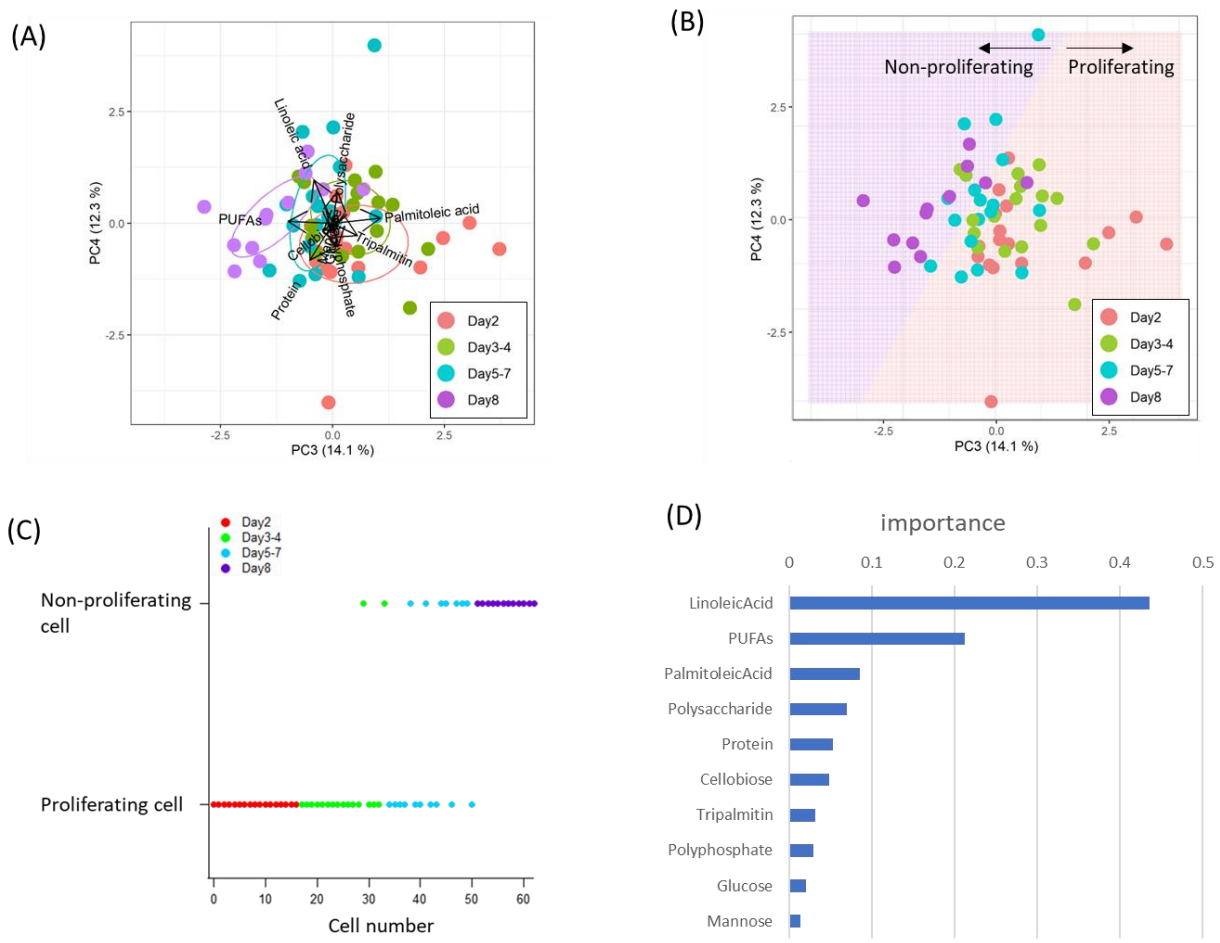

Figure 4. Classification of molecular profiling with growth phase in *C. tenuissimus*. (A) Principal Components Analysis (PCA) of the signal intensity of each biomolecular component. (B) Support Vector Machine analysis (SVM) of the grouping of proliferating and non-proliferating cells. (C) Random Forest analysis of two classified cells, including non-proliferating and proliferating. (D) Major components based on the classification are linoleic acid, polyunsaturated fatty acids, and palmitoleic acid.

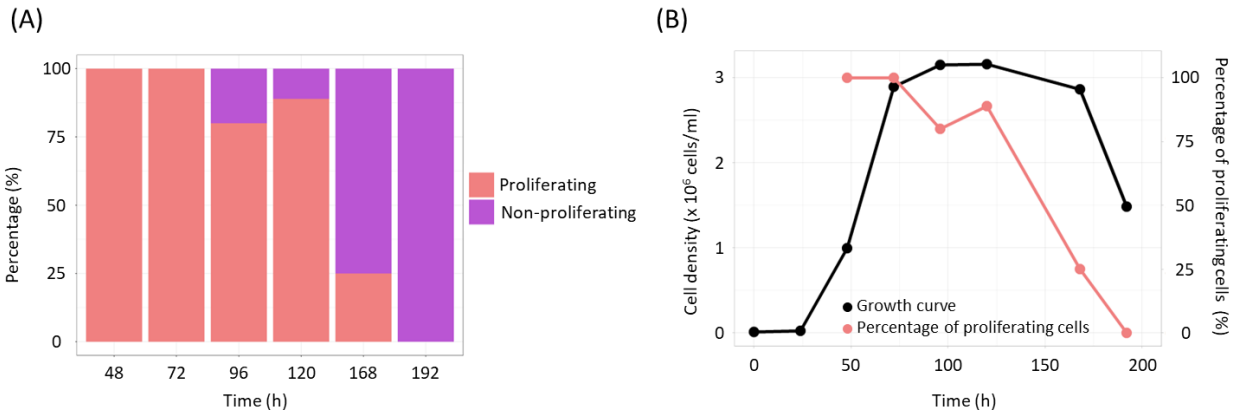

Figure 5. The growth phase differences between proliferating and non-proliferating cells of *C. tenuissimus* at single-cell levels over time. (A) Changes between proliferating and non-proliferating cells during 24 to 192 h after the incubation of *C. tenuissimus.* (B) The comparison between growth curve and percentage of proliferating cells of *C. tenuissimus.*

References

(1) Zohdi, E.; Abbaspour, M. Harmful Algal Blooms (Red Tide): A Review of Causes, Impacts and Approaches to Monitoring and Prediction. International Journal of Environmental Science and Technology 2019, 16 (3), 1789–1806.

(2) Tréguer, P.; Nelson, D. M.; Van Bennekom, A. J.; Demaster, D. J.; Leynaert, A.; Quéguiner, B. The Silica Balance in the World Ocean: A Reestimate. Science (1979) 1995, 268 (5209).

(3) States, P. Transcriptional Responses of the Marine Planktonic Diatom Chaetoceros Tenuissimus to Nitrogen- And. 2022, 56 (3), 295–301.

(4) Hano, T.; Tomaru, Y. Metabolomics-Based Approach to Explore Growth Phase-Dependent Markers in Cultured Diatom Chaetoceros Tenuissimus. J Chromatogr B Analyt Technol Biomed Life Sci 2019, 1128 (August), 121779.

(5) Hano, T.; Tomaru, Y. Metabolomics-Based Approach to Explore Growth Phase-Dependent Markers in Cultured Diatom Chaetoceros Tenuissimus. J Chromatogr B Analyt Technol Biomed Life Sci 2019, 1128 (August), 121779.

(6) Fiorini, F.; Borgonuovo, C.; Ferrante, M. I.; Brönstrup, M. A Metabolomics Exploration of the Sexual Phase in the Marine Diatom Pseudo-Nitzschia Multistriata. Mar Drugs 2020, 18 (6).

(7) Xu, Q.; Cui, Z.; Chen, N. Comparative Analysis of Chloroplast Genomes of Seven Chaetoceros Species Revealed Variation Hotspots and Speciation Time. Front Microbiol 2021, 12.

(8) He, S.; Xie, W.; Zhang, P.; Fang, S.; Li, Z.; Tang, P.; Gao, X.; Guo, J.; Tlili, C.; Wang, D. Preliminary Identification of Unicellular Algal Genus by Using Combined Confocal Resonance Raman Spectroscopy with PCA and DPLS Analysis. Spectrochim Acta A Mol Biomol Spectrosc 2018, 190, 417–422.

(9) Osterrothová, K.; Culka, A.; Němečková, K.; Kaftan, D.; Nedbalová, L.; Procházková, L.; Jehlička, J. Analyzing Carotenoids of Snow Algae by Raman Microspectroscopy and High-

Performance Liquid Chromatography. Spectrochim Acta A Mol Biomol Spectrosc 2019, 212, 262–271.

(10) Horii, S.; Ando, M.; Samuel, A. Z.; Take, A.; Nakashima, T.; Matsumoto, A.; Takahashi, Y. K.; Takeyama, H. Detection of Penicillin G Produced by Penicillium Chrysogenum with Raman Microspectroscopy and Multivariate Curve Resolution-Alternating Least-Squares Methods. J Nat Prod 2020, 83 (11), 3223–3229.

(11) Sugiyama, K.; Marzi, J.; Alber, J.; Brauchle, E. M.; Ando, M.; Yamashiro, Y.; Ramkhelawon, B.; Schenke-Layland, K.; Yanagisawa, H. Raman Microspectroscopy and Raman Imaging Reveal Biomarkers Specific for Thoracic Aortic Aneurysms. Cell Rep Med 2021, 2 (5), 100261.

(12) Samuel, A. Z.; Sugiyama, K.; Takeyama, H. Direct Intracellular Detection of Biomolecule Specific Bound-Water with Raman Spectroscopy. Spectrochim Acta A Mol Biomol Spectrosc 2023, 285 (June 2022), 121870.

(13) Yamaguchi, H.; Inoue, M.; Tanimoto, Y.; Sumida, N.; Adachi, M.; Kimura, K.; Tomaru, Y. Transcriptional Responses of the Marine Planktonic Diatom Chaetoceros Tenuissimus to Nitrogen-and Phosphorus-Deficient States.

(14) Chen, L. C. ‐ M; Edelstein, T.; McLachlan, J. BONNEMAISONIA HAMIFERA HARIOT IN NATURE AND IN CULTURE. J Phycol 1969, 5 (3).

(15) Ando, M.; Hamaguchi, H. Molecular Component Distribution Imaging of Living Cells by Multivariate Curve Resolution Analysis of Space-Resolved Raman Spectra. J Biomed Opt 2013, 19 (1), 011016.

(16) Hoyer, P. O. Non-Negative Matrix Factorization with Sparseness Constraints. Journal of Machine Learning Research 2004, 5, 1457–1469.

(17) Noothalapati, H.; Sasaki, T.; Kaino, T.; Kawamukai, M.; Ando, M.; Hamaguchi, H. O.; Yamamoto, T. Label-Free Chemical Imaging of Fungal Spore Walls by Raman Microscopy and Multivariate Curve Resolution Analysis. Sci Rep 2016, 6 (May), 1–10.

(18) Chiovitti, A.; Molino, P.; Crawford, S. A.; Teng, R.; Spurck, T.; Wetherbee, R. The Glucans Extracted with Warm Water from Diatoms Are Mainly Derived from Intracellular Chrysolaminaran and Not Extracellular Polysaccharides. Eur J Phycol 2004, 39 (2), 117–128.

(19) Huang, W. E.; Griffiths, R. I.; Thompson, I. P.; Bailey, M. J.; Whiteley, A. S. Raman Microscopic Analysis of Single Microbial Cells. Anal Chem 2004, 76 (15), 4452–4458.

(20) Majed, N.; Matthäus, C.; Diem, M.; Gu, A. Z. Evaluation of Intracellular Polyphosphate Dynamics in Enhanced Biological Phosphorus Removal Process Using Raman Microscopy. Environ Sci Technol 2009, 43 (14), 5436–5442.

(21) PRATIWI, A. R.; SYAH, D.; HARDJITO, L.; PANGGABEAN, L. M. G.; SUHARTONO, M. T. Fatty Acid Synthesis by Indonesian Marine Diatom, Chaetoceros Gracilis. Hayati 2009, 16 (4), 151–156.